REGULAR PAPER

A Simplified Anisotropic Yield Function not Requiring Parameter Optimization for Sheet Metals

Jae-Hyuk Lim[1] · Eun-Ho Lee[1,2]

Abstract

Recently developed anisotropic yield functions can capture the material anisotropic behaviors through parameter optimization. However, sometimes the parameter optimization is not easy and does not always have a unique solution. This paper introduces an anisotropic yield function that does not require the parameter calibration process. This model simplifies the coupled quadratic and non-quadratic yield function in order to directly use the measured on-set of yielding stress and r-value data without the calibration process. The presented model is validated with five different materials for the prediction of stress and strain anisotropies. In addition, a cup drawing simulation is also presented to validate the simplified model in a practical metal forming simulation with the User-defined subroutine of ABAQUS. The results of this paper show that the simplified model can be effectively employed for the simulation of sheet metal forming processes.

Keywords Anisotropy · Non-associated flow rule · Yield function · Cup drawing · Finite element method

1 Introduction

Yield function plays an important role to predict the yielding condition of materials and the anisotropic properties. The first anisotropic yield function was introduced by Hill [1], in 1948, with a quadratic form using 6 anisotropic parameters to predict the anisotropic mechanical properties. However, the Hill1948 model can have only one curvature of the yield surface and thus not consider the crystalline structure of materials. Independently, Hosford [2], in 1972, developed an isotropic non-quadratic yield function that can control the curvature of the yield surface. Later, Hill generalized the anisotropic yield function based on the Hill1948 model to consider the crystalline structures in 1972 and 1990 [3, 4]. Hosford also came up with an extended model to consider the anisotropic properties by introducing anisotropic parameters [5, 6]. These models have been the basis of the study of anisotropic yield functions. However, they cannot satisfy both stress and strain (r-value) anisotropic properties

at the same time due to insufficient numbers of the material coefficients in the models. Since then, many researchers have been trying to include more material constants to describe stress and strain anisotropies [7–12]. One of the most widely used models is the Yld2000-2d model, introduced by Barlat et al. [13], which can describe stress and r-value anisotropies by optimizing 8 parameters for the measured yield stresses and r-values at 0°, 45°, and 90° to the rolling direction (RD) and the equal biaxial (EB) condition, respectively. In parallel, Banabic et al., [14] proposed the BBC2003 model, which consider the shear effect based on Barlat and Lian 1989 model [7]. Later Banabic et al., [15] presented an improved version, the BBC2005, by rearranging the anisotropic coefficients. Cazacu et al., [16] also proposed a yield function to capture the strength-differential effect (SDE). The aforementioned models are based on the associated flow rule (AFR), which uses a yield function as a plastic potential to obtain the direction of plastic strain rate. The AFR has provided good numerical solutions for sheet metal forming processes. In parallel with the AFR, some researchers have studied a non-associated flow rule (non-AFR) by employing an additional function as a plastic potential which defines the direction of plastic strain rate [17]. One of the widely used methods is to employ two separated quadratic functions [18–23], and this method is also very effective at capturing both stress and r-value anisotropies. However, one limitation

✉ Eun-Ho Lee
e.h.lee@skku.edu

[1] Department of Mechanical Engineering, Sungkyunkwan University, Suwon, Gyeonggi-do 16419, Republic of Korea

[2] Department of Smart Fab. Technology, Sungkyunkwan University, Suwon, Gyeonggi-do 16419, Republic of Korea

is that this method cannot control the curvature of the yield function. A recently introduced model by coupling of quadratic and non-quadratic (CQN) functions [24] can control the curvature of the yield surface and also capture the anisotropic behavior under the non-AFR, so that it has shown good agreements with experimental data [25–27]. However, the CQN model requires multiple data sets for the evolving history of the yield surface according to plastic hardening, and it also requires parameter calibration for different stress states. Even though the CQN model provides good numerical solutions, in many cases, especially in the industry use, it is not easy to prepare all data required to perform calibration for different stress states. The other models mentioned above also require the optimization of the model parameters. However, sometimes parameter optimization is not easy and does not always have a unique solution. For convenience of use and accessibility of data, it will be useful to employ an anisotropic yield function that does not require the parameter optimization with less data.

This paper presents an anisotropic yield function that does not require parameter optimization. This model simplifies the anisotropic parameters of the CQN yield model to avoid the calibration process and then, by substituting the measured on-set of yield stress values and r-values into the function, the model represents the stress and strain anisotropies. The simplified yield model (hereinafter called as the new model) is implemented into the User-defined MATerial (UMAT) subroutine of the ABAQUS program and validated with AA6022-T43, AA5182-O, AA6181-T4, MP980, and 718AT metal sheets to predict stress and strain anisotropies. In addition, a cup drawing simulation is conducted to test the new model in a practical metal forming condition. The results of this paper show that the new model can be effectively used for simulation of sheet metal forming processes without model calibration process. The outline of this paper is following. The formulation of the new model is introduced in Sect. 2, and Sect. 3 represents the ability of the new model. Section 4 shows the cup drawing simulation and the conclusion is in Sect. 5.

2 Modeling

2.1 Brief Description of Material Dissipation

Section 2.1 briefly introduces the basic equations for material dissipation to formulate the yield function. The inequality of material dissipation rate under small deformation condition is given by [28]

$$\xi = \boldsymbol{\sigma} : \dot{\boldsymbol{\varepsilon}} - \dot{\overline{\psi}}(\rho, \psi) \geq 0 \tag{1}$$

where $\boldsymbol{\sigma}$ is the Cauchy stress and $\dot{\boldsymbol{\varepsilon}}$ is the strain rate. $\dot{\overline{\psi}}$ denotes the rate of free energy change, affected by the material density (ρ) and the Helmholtz free energy density (ψ). In the isothermal condition, the free energy of a linear elastic material can be given by

$$\overline{\psi} = \frac{1}{2}\boldsymbol{\varepsilon}^e : C : \boldsymbol{\varepsilon}^e \quad \text{where} \quad \boldsymbol{\varepsilon}^e = \boldsymbol{\varepsilon} - \boldsymbol{\varepsilon}^p \tag{2}$$

where $\boldsymbol{\varepsilon}$ is total strain, $\boldsymbol{\varepsilon}^e$ denotes elastic strain, and $\boldsymbol{\varepsilon}^p$ means plastic strain. **C** is the linear elastic stiffness tensor. Since the Cauchy stress and rate of free energy change are given by

$$\boldsymbol{\sigma} = \frac{\partial \overline{\psi}}{\partial \varepsilon^e} \quad \text{and} \quad \dot{\overline{\psi}} = \frac{\partial \overline{\psi}}{\partial \varepsilon^e} : \dot{\varepsilon}^e \tag{3}$$

Based on Eq. (3), the material dissipation rate of Eq. (1) should satisfy

$$\xi = \boldsymbol{\sigma} : \dot{\boldsymbol{\varepsilon}}^p \geq 0 \tag{4}$$

2.2 Plastic Flow

From Eq. (4), the plastic flow rule defines the rate of plastic strain [17]

$$\dot{\boldsymbol{\varepsilon}}^p = \frac{\partial \phi_p(\sigma)}{\partial \sigma} \dot{\overline{\varepsilon}}^p \tag{5}$$

where ϕ_p is a plastic potential and $\dot{\overline{\varepsilon}}^p$ is the rate of effective plastic strain. If ϕ_p is a convex function of stress, the inequality condition of the material dissipation rate in (4) is satisfied. In determining the form of ϕ_p, there are generally two choices either AFR or non-AFR. This paper uses the non-AFR. Next, in order to consider the anisotropy of plastic strain, the material orthotropic axes $\boldsymbol{\mu}_i$ are defined

$$\boldsymbol{\mu}_i = \boldsymbol{\Omega} \boldsymbol{\mu}_i(0), \quad \det(\boldsymbol{\Omega}) = 1, \quad \boldsymbol{\Omega}\boldsymbol{\Omega}^T = \mathbf{I}, \quad \boldsymbol{\Omega}^T = -\boldsymbol{\Omega}, \quad (\text{for} \quad i = 1, 2, 3) \tag{6}$$

$\boldsymbol{\mu}_i(0)$ is the initial material axes and $\boldsymbol{\Omega}$ is a proper orthogonal tensor to describe the rotation of the material axes. For the evolution of the rotation tensor $\boldsymbol{\Omega}$, this work uses the minimum plastic work theory with the decomposed rotational tensor from the deformation gradient [29, 30]. The components of the Cauchy stress (σ_{ij}) and strain (ε_{ij}) can be defined on the orthotropic material axes, and the tensors are given by

$$\boldsymbol{\sigma} = \sigma_{ij}\boldsymbol{\mu}_i \otimes \boldsymbol{\mu}_j \quad and \quad \boldsymbol{\varepsilon} = \varepsilon_{ij}\boldsymbol{\mu}_i \otimes \boldsymbol{\mu}_j \tag{7}$$

In this paper, the Hill1948 model is used as the plastic potential, ϕ_p, under the plane stress assumption. because this model can effectively describe the strain anisotropy. Under the plane stress condition considering sheet metal forming, the plastic potential function is given as below [17]:

$$\phi_p = \sqrt{\sigma_{11}^2 + \lambda_p \sigma_{22}^2 - 2v_p \sigma_{11}\sigma_{22} + 2\rho_p \sigma_{12}\sigma_{12}} \qquad (8)$$

where σ_{11} and σ_{22} are normal stress components and σ_{12} is shear stress component in the plane stress condition. Here, the three strain anisotropic parameters can be defined as below:

$$\lambda_p = \frac{r_0(r_{90}+1)}{r_{90}(r_0+1)}, \quad v_p = \frac{r_0}{r_0+1}, \quad \rho_p = \frac{(1+2r_{45})(r_0+r_{90})}{2r_{90}(r_0+1)} \qquad (9)$$

r_0, r_{45}, and r_{90} are the measured r-values in three directions (0°, 45°, and 90°) based on the RD.

2.3 An Simplified CQN Yield Function

Next the yield condition is generally defined as below:

$$F(\sigma, \overline{\varepsilon}^p) = f(\sigma) - \overline{\sigma}(\overline{\varepsilon}^p) \qquad (10)$$

If $F\left(\sigma, \overline{\varepsilon}^P\right) < 0$, the material is within elastic range, but the elastic–plastic condition makes that $F\left(\sigma, \overline{\varepsilon}^P\right) = 0$. $f(\sigma)$ represents the yield surface and $\overline{\sigma}(\overline{\varepsilon}^p)$ is the hardening curve at a reference direction, which is set to the rolling direction (RD) in this paper. $f(\sigma)$ is specified by

Fig. 1 An example of effect of exponent value on the yield surface

as the ratio of initial stresses with respect to the loading direction at the on-set of the yielding condition,

$$\alpha_1 = \left(\frac{\overline{\sigma}_0}{\overline{\sigma}_{90}}\right)^{n+2}, \quad \alpha_2 = \left(\frac{\overline{\sigma}_0}{\overline{\sigma}_{EB}}\right)^{n+2}, \text{ and } \alpha_3 = \left(\frac{\overline{\sigma}_0}{\overline{\sigma}_{45}}\right)^{n+2} \qquad (12)$$

$$f(\boldsymbol{\sigma}) = \left\{ \begin{array}{l} [(\sigma_{11} - \alpha_1\sigma_{22})(\sigma_{11} - \sigma_{22}) + \alpha_2(\sigma_{11}\sigma_{22} - \sigma_{12}\sigma_{12}) + 4\alpha_3\sigma_{12}^2] \\ \times \left[\frac{1}{2}\left(|\sigma_1|^n + |\sigma_2|^n + |\sigma_1 - \sigma_2|^n\right)\right] \end{array} \right\}^{\frac{1}{n+2}} \qquad (11)$$

The form of Eq. (11) is the coupling of quadratic and non-quadratic functions [24]. The non-quadratic part $[\frac{1}{2}(|\sigma_1|^n + |\sigma_2|^n + |\sigma_1 - \sigma_2|^n)]$ can change the curvature of the yield surface to consider the crystalline structure, while the role of quadratic part $[(\sigma_{11} - \alpha_1\sigma_{22})(\sigma_{11} - \sigma_{22}) + \alpha_2(\sigma_{11}\sigma_{22} - \sigma_{12}\sigma_{12}) + 4\alpha_3\sigma_{12}^2]$ is to capture the anisotropy of yield stresses by the anisotropic parameters (α_1, α_2, and α_3); the anisotropic parameters are defined in Eq. (12). n is the exponent to control the curvature of the yield surface, which is depending on the crystallographic structure as shown in Fig. 1. The role of the exponent n is the same to that of other models [13–24]. The combination of two parts can take advantage of each part by capturing both anisotropy and curvature change of yield surface affected by the crystalline structure. In the quadratic part, the anisotropic parameters (α_1, α_2, and α_3) should be specified to account for the stress anisotropy of materials. To use this model without the parameter calibration process, the anisotropic parameters are simply defined
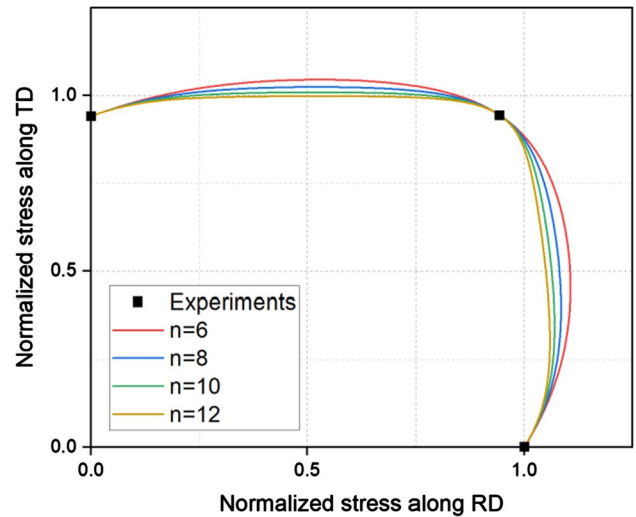
$\overline{\sigma}_0$, $\overline{\sigma}_{45}$, $\overline{\sigma}_{90}$, and $\overline{\sigma}_{EB}$ are the measured on-set of yield stresses for three directions (0°, 45°, and 90°) and EB condition, respectively. α_1, α_2, and α_3 reflect the ratio of $\overline{\sigma}_{90}$, $\overline{\sigma}_{45}$, and $\overline{\sigma}_{EB}$ to $\overline{\sigma}_0$ in the yield surface to describe the anisotropic shape of the yield surface. Unlike other models, optimization of the anisotropy parameters is not required. This model directly uses the measured r-values and yield stresses in Eqs. (8) and (12), respectively, without the calibration process. Figure 1 shows the effect of the exponent n of the curvature of the yield surface. Note that the data of AA6022-T43 (in Table 2) are used for this example of Fig. 1. In this work, the n value for three aluminum materials (AA6022-T43, AA5082-O, and AA6181-T4) is 10, and the others (MP980 and 718AT) have 6 for the n value. In order to obtain the rate of effective plastic strain, $\dot{\overline{\varepsilon}}^p$, the yield consistency (13a), stress rate (13b), and hardening slop (13c) relations are used with Eqs. (2) and (5), respectively,

$$\dot{F} = \frac{\partial f}{\partial \sigma_{ij}}\dot{\sigma}_{ij} - H\dot{\overline{\varepsilon}}^p = 0 \qquad (13a)$$

Table 1 Hardening parameters from the RD for the four materials

Materials	Hardening parameters				
	A [MPa]	B [MPa]	C [−]	b [−]	D [MPa]
AA6022-T43	338.86	202.29	10.38	1.00	0.42
AA5182-O	366.75	250.97	11.18	1.00	0.23
MP980	1011.98	371.15	52.99	0.79	1114.29
718AT	529.54	318.34	9.79	1.00	6.17

$$\dot{\sigma}_{ij} = C_{ijkl}\dot{\varepsilon}_{kl} - C_{ijkl}\frac{\partial \phi_p}{\partial \sigma_{kl}}\dot{\bar{\varepsilon}}^{\,p} \tag{13b}$$

$$H = \frac{d\bar{\sigma}_0}{d\bar{\varepsilon}^p} \tag{13c}$$

Finally, the rate of the effective plastic strain is obtained by

$$\dot{\bar{\varepsilon}}^{\,p} = \chi\frac{\frac{\partial f}{\partial \sigma_{ij}}C_{ijkl}\dot{\varepsilon}_{kl}}{\frac{\partial f}{\partial \sigma_{ij}}C_{ijkl}\frac{\partial \phi_p}{\partial \sigma_{kl}}} \tag{14}$$

χ is a switch parameter having either 1 or 0. $\chi = 1$ when $F(\boldsymbol{\sigma}, \bar{\varepsilon}^p) = 0$ and $\frac{\partial f}{\partial \sigma_{ij}}C_{ijkl}\dot{\varepsilon}_{kl} > 0$. Otherwise $\chi = 0$.

3 Model Validation

3.1 Material Properties

The presented model is verified for the five material data sets (AA6022-T43 [21], AA5182-O [21], AA6181-T4 [14],

MP980 [24], and 718AT [21] sheet metals). In order to conduct metal forming simulation, the hardening curve, $\bar{\sigma}(\bar{\varepsilon}^p)$, in Eq. (10) should also be specified. A modified Hockett-Sherby model is used in this work.

$$\bar{\sigma}(\bar{\varepsilon}^p) = A - B\exp\left(-C(\bar{\varepsilon}^p)^b\right) + D\bar{\varepsilon}^p \tag{15}$$

The hardening constants (A, B, C, b, and D) are determined based on the RD hardening. The parameters of the modified Hockett-Sherby model are listed in Table 1, and the initial yield stress for all materials are listed in Table 2. Note that AA6181-T4 data are excluded in Table 1 because it does not have the hardening data but the on-set of yield stress in Table 2. The r-values are shown in Table 3. The data for directions of 15°, 30°, 60°, and 75° are not necessary to determine the shape of the yield surface, but used in the validation of the new model in Sect. 3.2. Figure 2 presents the yield and plastic potential surfaces of the new model in the plane stress space for the five materials. The red and blue surfaces are for the yield function f and plastic potential function ϕ_p, respectively, in each figure. In each 3D yield surface, the red line denotes the uniaxial stress state, and the blue line presents the yield surface on the normal plane consisting of the RD and the transverse direction (TD). As shown in Fig. 2, the surfaces are convex to satisfy the inequality condition of the material dissipation in Eq. (4).

3.2 Anisotropy in Strain and Stress

To verify the new model for stress and strain anisotropies, normalized stress ratio and r-value were analyzed. The normalized stress ratio is the yield stress that changes along

Table 2 Initial yield stress at intervals of 15 degrees for the five materials

Materials	Initial yield stress							
	$\bar{\sigma}_0$	$\bar{\sigma}_{15}$	$\bar{\sigma}_{30}$	$\bar{\sigma}_{45}$	$\bar{\sigma}_{60}$	$\bar{\sigma}_{75}$	$\bar{\sigma}_{90}$	$\bar{\sigma}_{EB}$
AA6022-T43	136.57	137.31	137.72	136.12	133.87	130.88	128.49	128.85
AA5182-O	115.78	114.11	112.89	111.65	110.83	112.16	114.28	125.22
AA6181-T4	142	–	–	138	–	–	137	134
MP980	640.83	653.56	631.25	598.82	579.91	577.72	617.32	582.97
718AT	211.2	212.99	213.21	219.42	224.74	222.13	216.51	237.88

Table 3 r-values at intervals of 15 degrees for the five materials

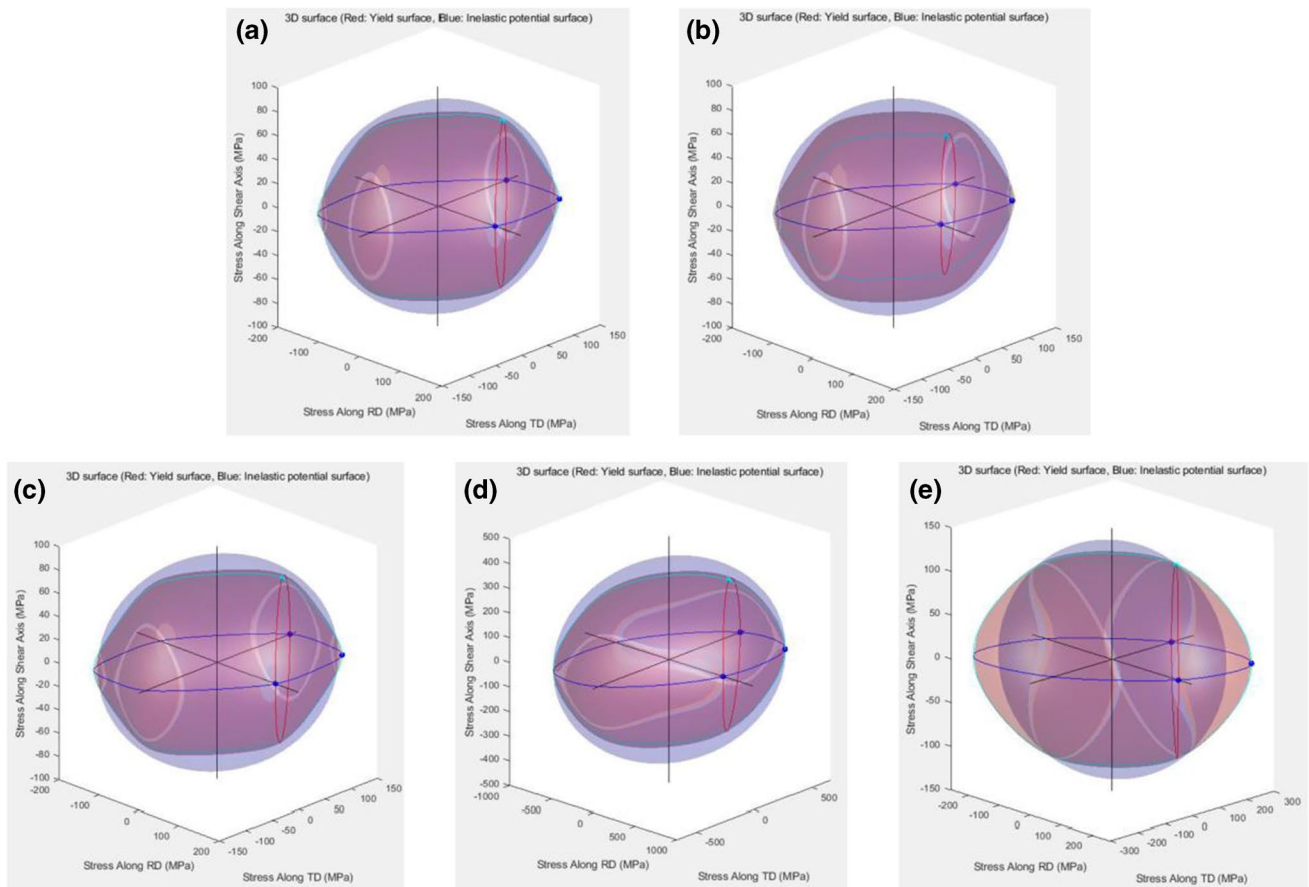| Materials	r-values							
	r_0	r_{15}	r_{30}	r_{45}	r_{60}	r_{75}	r_{90}	r_{EB}
AA6022-T43	1.029	1.010	0.703	0.532	0.553	0.689	0.728	1.149
AA5182-O	0.957	0.903	0.916	0.934	0.947	0.981	1.058	0.948
AA6181-T4	0.672	–	–	0.606	–	–	0.821	0.820
MP980	0.810	0.845	0.925	0.995	1.015	1.035	1.058	0.977
718AT	1.830	1.763	1.834	2.294	2.708	2.562	2.517	0.803

Fig. 2 Yield and plastic potential surfaces of the new model in the plane stress space for the five materials; **a** AA6022-T43; **b** AA5182-O; **c** AA6181-T4; **d** MP980; **e** 718AT

the load direction, and it is normalized by the yield stress of the reference direction ($\overline{\sigma}_0$). The r-value is a standard measurement to evaluate the strain anisotropy in the metal sheet ([15, 17], and [27]). It is defined as the ratio of width strain to thickness strain,

$$r_\theta = \frac{\varepsilon^p_{width}}{\varepsilon^p_{thickness}} = -\frac{\varepsilon^p_{11}\sin^2(\theta) + \varepsilon^p_{22}\cos^2(\theta) - 2\varepsilon^p_{12}\cos(\theta)\sin(\theta)}{\varepsilon^p_{11} + \varepsilon^p_{22}}$$

(16)

Due to the zero dilatancy condition of plastic deformation, the strain in the thickness direction can be given by $\varepsilon^p_{thickness} = \varepsilon^p_{33} = -\left(\varepsilon^p_{11} + \varepsilon^p_{22}\right)$, and the strain in the width direction can be defined $\varepsilon^p_{width} = \varepsilon^p_{11}\sin^2(\theta) + \varepsilon^p_{22}\cos^2(\theta) - 2\varepsilon^p_{12}\cos(\theta)\sin(\theta)$ with considering strain transformation. θ denotes the loading direction with respect to the reference direction. The verification results for strain and stress anisotropies are in Figs. 3 and 4, respectively, for the five materials (AA6022-T43, AA5182-O, AA6181-T4, MP980, and 718AT). All the measured values (black square symbols) are at intervals of 15 degrees, and the new model (blue line) represents a

continuous distribution; the new model is also compared to other models, the CQN2017 [24] (red dashed line) and the Yld2000-2d [13] (green dotted line). If the material is isotropic, r-value and normalized stress ratio had a constant value (black dashed line) in Figs. 3 and 4.

Figure 3a–e show the r-value distributions of the three models for the five materials. The aluminum materials are shown in Fig. 3a–c. AA6022-T43 has quite a large deviation from RD to TD, but the AA5182-O and AA6181-T4 show relatively smaller deviations. For the MP980 and 718AT materials shown in Fig. 3d–e, the new model shows a similar change in the r-value distribution. The new model correctly passes the measured r-values in the three major directions (0°, 45°, and 90°). Even though the other angles (15°, 30°, 60°, and 75°) lead to some errors, the presented model can follow the tendency of the r-value change for all of the materials. Figure 4a–e represents the normalized stress ratio for the same materials and models. The magnitude of distribution of the stress anisotropy has a narrower range than that of the r-value. Similar to the strain anisotropy, the new model correctly passes the measured data in the three
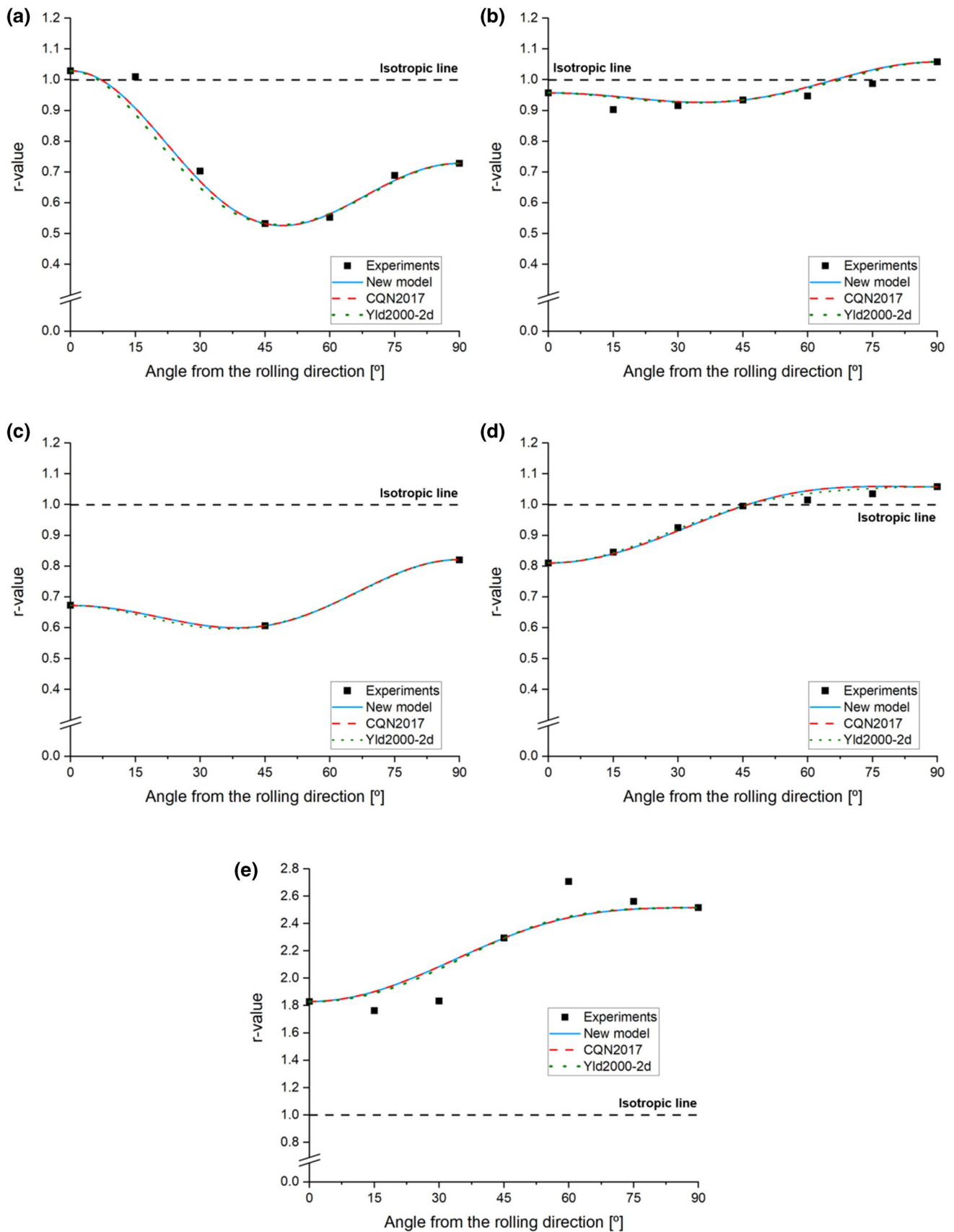
Fig. 3 Prediction of the r-values of the three models for the five materials; **a** AA6022-T43; **b** AA5182-O; **c** AA6181-T4; **d** MP980; **e** 718AT
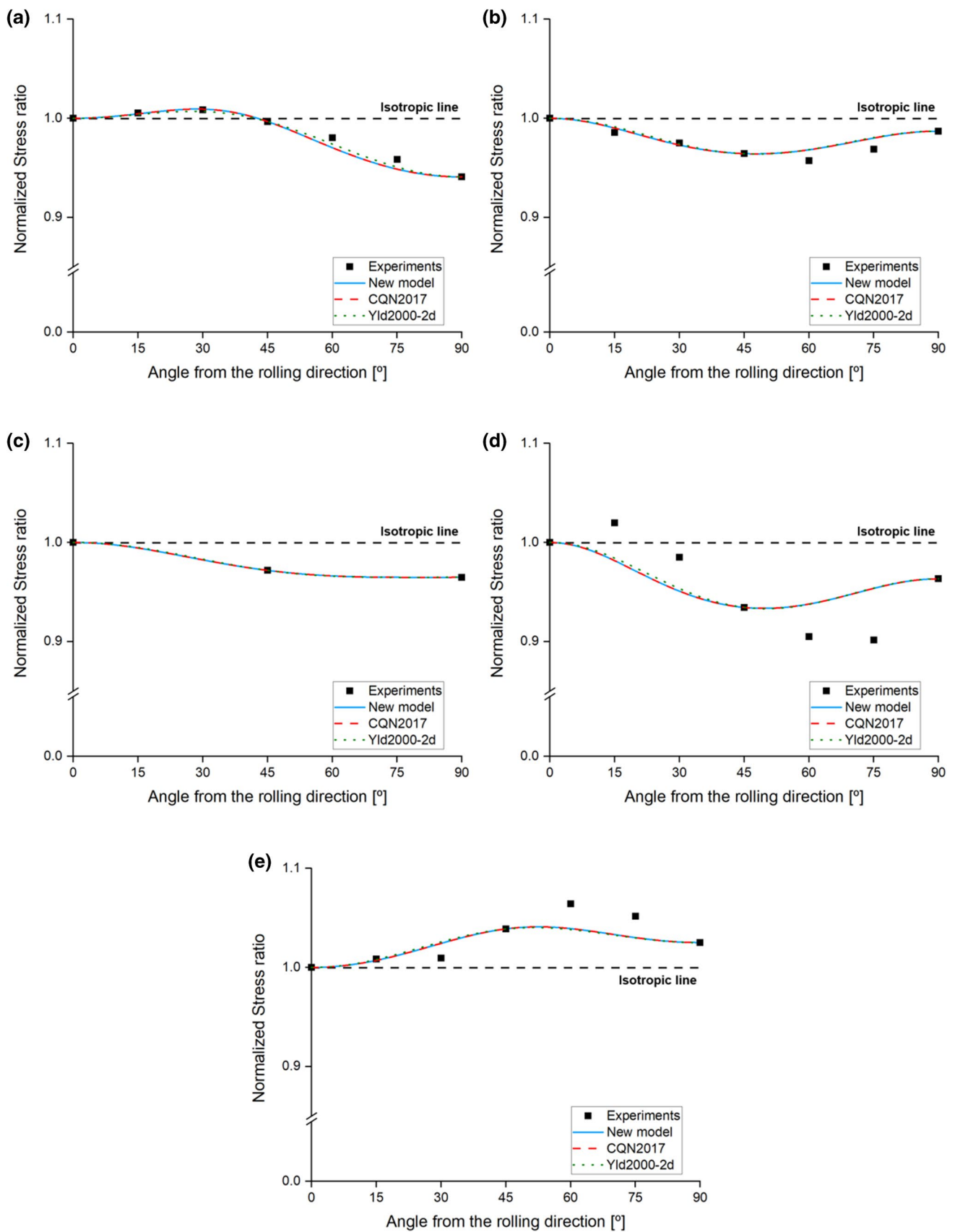
Fig. 4 Prediction of the normalized stress ratio of the three models for the five materials; **a** AA6022-T43; **b** AA5182-O; **c** AA6181-T4; **d** MP980; **e** 718AT

main directions (0°, 45°, and 90°), and follows the tendency of the anisotropy change well. As shown in Figs. 3 and 4, the new model can provide almost the same performance as the CQN2017 and Yld2000-2d models in prediction of the r-value and stress anisotropies. For a quantitative estimation of the anisotropies in strain and stress, the root mean square (RMS) errors for the r-value and normalized stress ratio are shown in Fig. 5. Note that the AA6181-T4 data has no error in both anisotropy distributions because it has only data for the three main directions (0°, 45°, and 90°). The accuracy of the three models is very similar. The models show that errors of the r-value and normalized stress ratio of the five materials are less than 5% except for the r-value of the 718AT material. That's because the measured r-value at 30° and 60° of the 718AT material make strong inflections. Based on the validation results, the presented model provides good agreements with the measured r-value and stress anisotropies.

3.3 Yield Surface in the Normal Plane

In this section, the new model is verified for the yield surface compared with the other yield functions. Figure 6a–e shows the four yield surfaces with measured data on the normal plane for the five materials, and they are represented with different colors or symbols, e.g. the isotropic model (black line), new model (blue line), CQN2017 (red dashed line), Yld2000-2d (greed dotted line), and experiments for RD (purple square), TD (red square), and EB (green square), respectively. In the isotropic model, the measured yield stresses on TD and EB have some errors; the isotropic model is employed as a reference. However, the new model can capture the experimental data for the RD, TD, and EB condition, and has very similar contours

to the Yld2000-2d and CQN2017 models for all materials. In addition, the AA6181-T4 has extra biaxial tension data (black squares), and the models follow the additional data well. This performance of the model in capturing data is very acceptable compared to other reported models [13–15].

4 Cup Drawing Simulation

The previous section showed the verification of the new model. This section represents a cup drawing simulation with the Yld2000-2d, CQN2017, and new models by using the finite element (FE) method. The used program is ABAQUS explicit solver with the Vectorized-User MATerial (VUMAT) subroutine. In this study, the new model is compared to the CQN2017 and Yld2000-2d for AA6022-T43 material; the Yld2000-2d model has provided very good anisotropic prediction in the same problem [31, 32]. For the simulation conditions, the total punch stroke is 60 mm and the blank holding force (BHF) is set to 20kN. The quarter symmetric condition is applied to improve the efficiency of the finite element (FE) model, as shown in Fig. 7.

The effective stress results at 20 mm punch stroke are presented for three yield functions in Fig. 8. The results show that the new model can closely predict the effective stress contour compared to the Yld2000-2d and CQN2017 models. Figure 9 represents the cup height profiles of the three models at the end of stroke, and the models also provide very similar results. Consequently, the cup drawing analysis show that the new model can describe the effect of anisotropic behaviors in the metal forming simulation.
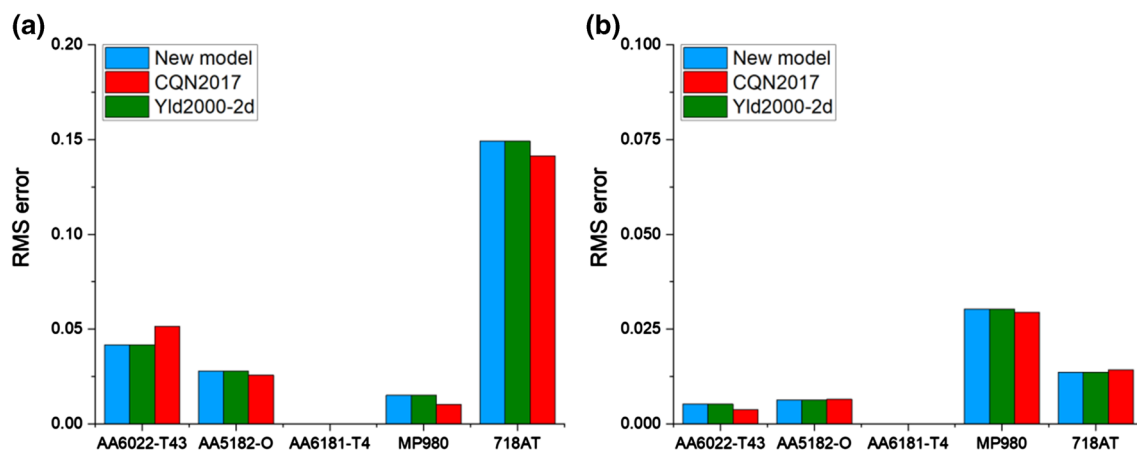

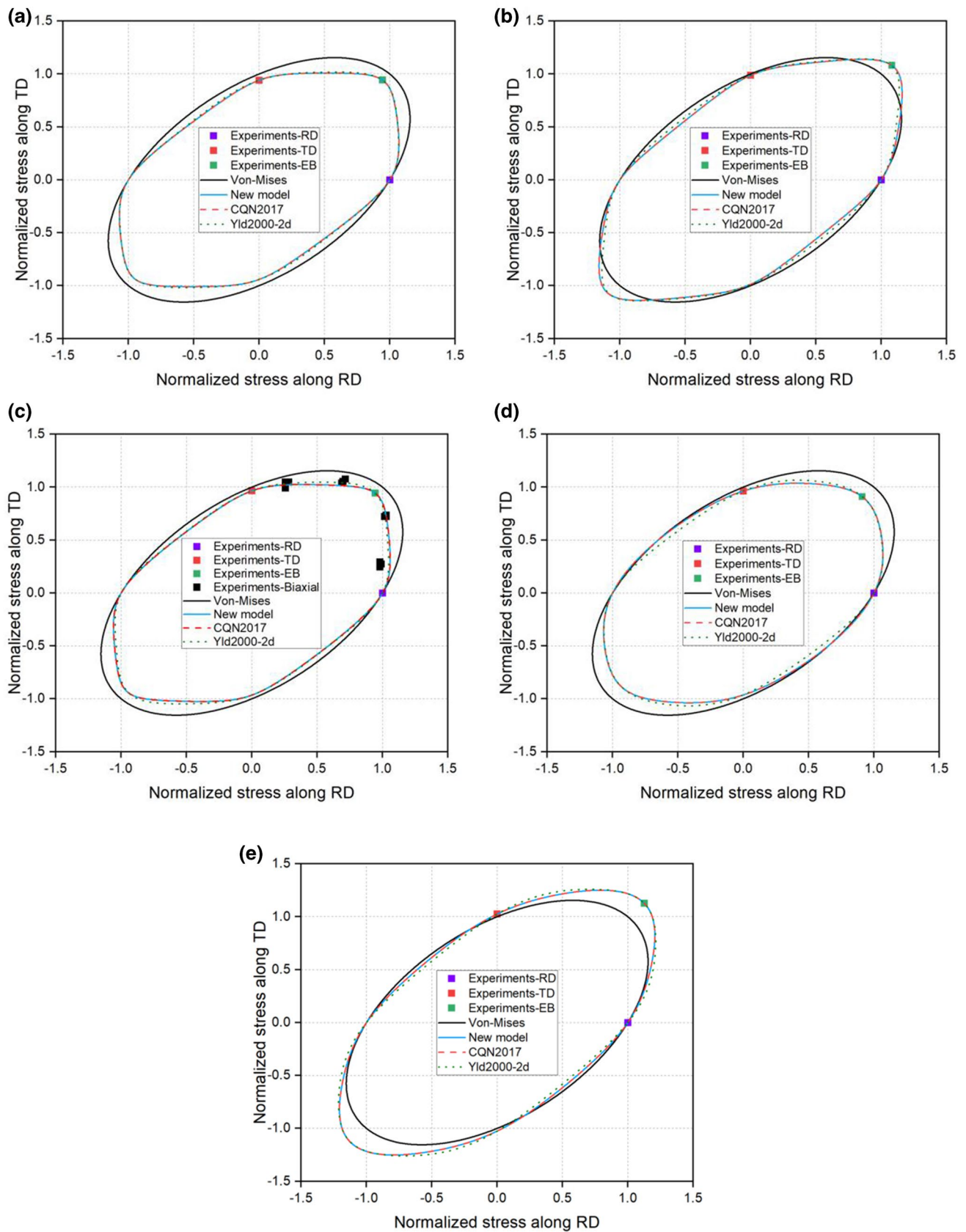**Fig. 5** RMS errors of the three models for the five materials; **a** r-value; **b** normalized stress ratio

Fig. 6 Normalized yield surfaces on the normal plane; **a** AA6022-T43; **b** AA5182-O; **c** AA6181-T4; **d** MP980; **e** 718AT
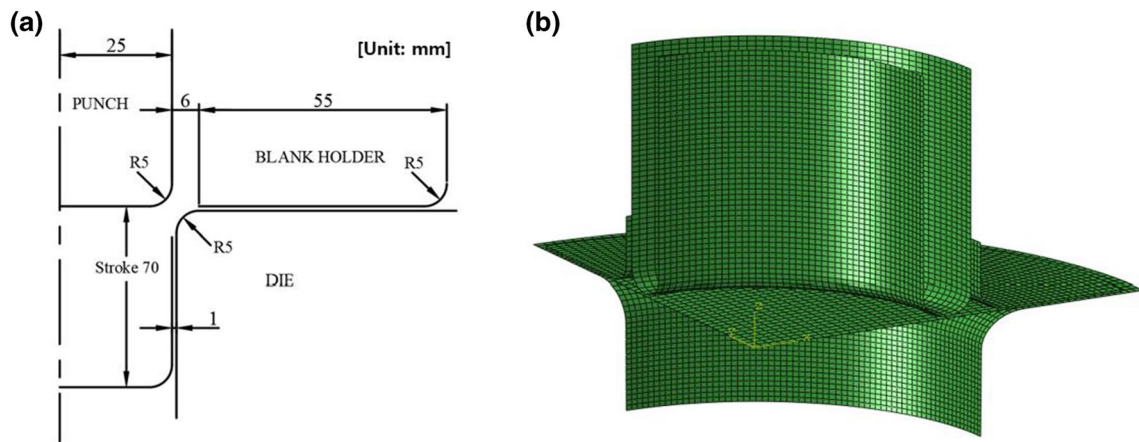
Fig. 7 FE model of a circular cup drawing; **a** 2D drawing; **b** FEM modeling
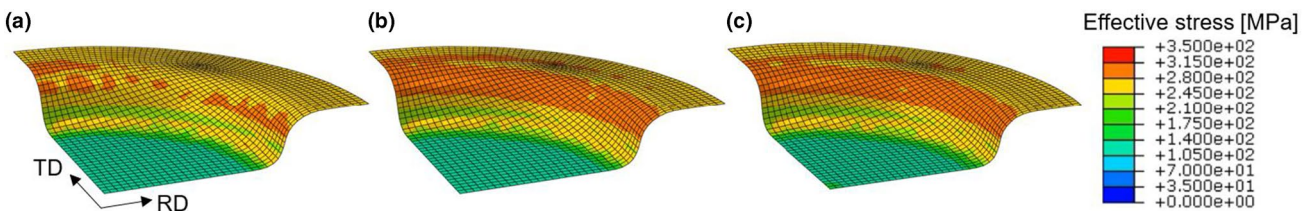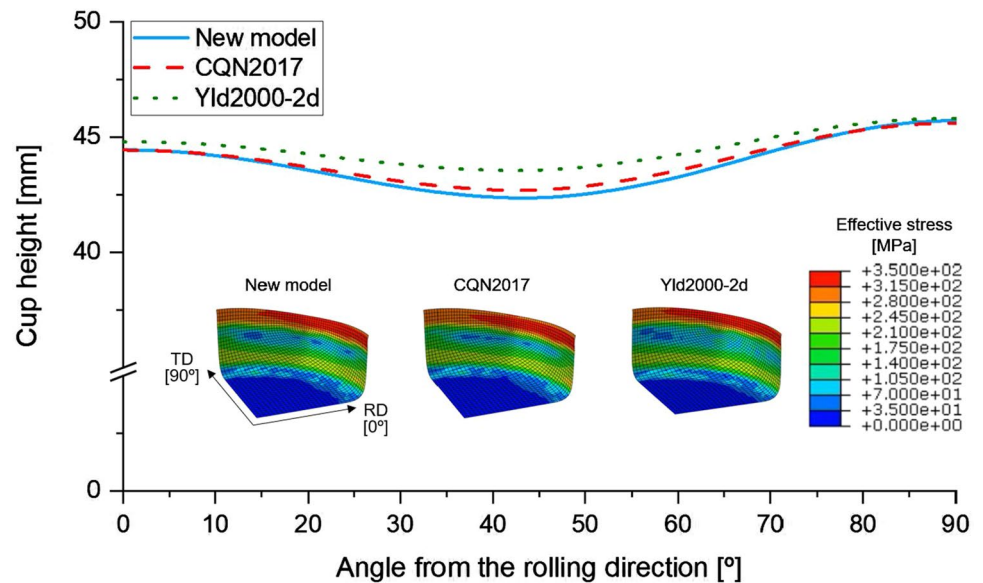

Fig. 8 Effective stress results at stroke 20 mm for the three yield functions; **a** CQN2017; **b** New model; **c** Yld2000-2d

Fig. 9 Results of cup height profiles at stroke 60 mm for the three yield models

5 Conclusion

In this work, a yield function not requiring parameter optimization is introduced. This model simplifies the anisotropic parameters of the CQN model in order to avoid parameter optimization. The new model was verified in previous sections from certain points of view, e.g. strain and stress anisotropy, the yield surface, and the cup drawing simulation. Results show good agreements with experiments. More details about the new model and specific results are below:

1. The new model is formulated under the Non-AFR, and simplifies the hardening history data of the CQN yield model. Since the new model directly uses the measured stresses and r-values for the anisotropic parameters, it does not require parameter optimization to determine the shape of yield surface.

2. The new model provides good predictions for stress and strain anisotropies. This model correctly passes the stress and r-value data at the three main directions (0°, 45°, and 90°), and it can follow the experimental tendency of the anisotropic change with respect to loading directions.

3. The new model can exactly capture the yield surface at the RD, TD, and EB condition by using the simplified anisotropic parameters (α_1, α_2, and α_3). Also, it can consider the different curvatures of the yield surface by controlling the exponent value.

4. The new model can provide almost the same performance as the Yld2000-2d and CQN2017 models in prediction of strain and stress anisotropies.

5. In the cup drawing simulation, the presented model describes very similar results for the stress contour and cup height profile compared to the Yld2000-2d and CQN2017 models.

Declarations

Conflict of interest The authors declare that there are no conflicts of interest.

References

1. Hill, R. (1948). A theory of the yielding and plastic flow of anisotropic metals. Proc. R. *Soc. Lond, A, 193*, 281–297.
2. Hosford, W. F. (1972). A generalized isotropic yield criterion. *J. Appl. Mech. Trans, 39*(2), 607–609.
3. Hill, R. (1972). Constitutive analysis of elastic-plastic crystals at arbitrary strain. *Journal of the Mechanics and Physics of Solids, 20*(6), 401–413.
4. Hill, R. (1990). Constitutive modelling of orthotropic plasticity in sheet metals. *Journal of the Mechanics and Physics of Solids, 38*(3), 405–417.
5. Hosford, W.F. (1979). On yield loci of anisotropic cubic metals. In: *Proc. 7th North American Metalworking Conf*. SME, Dearborn, MI.
6. Logan, R. W., & Hosford, W. F. (1980). Upper-bound anisotropic yield locus calculations assuming< 111>-pencil glide. *International Journal of Mechanical Sciences, 22*(7), 419–430.
7. Barlat, F., & Lian, J. (1989). Plastic behavior and stretchability of sheet metals. Part I: A yield function for orthotropic sheets under plane stress conditions. *Int. J. Plasticity, 5*, 51–66.
8. Barlat, F., Lege, D. J., & Brem, J. C. (1991). A six-component yield function for anisotropic materials. *Int. J. Plas, 7*(7), 693–712.
9. Chung, K., & Shah, K. (1992). Finite element simulation of sheet metal forming for planar anisotropic metals. *International Journal of Plasticity, 8*(4), 453–476.
10. Yoon, J. W., Yang, D. Y., Chung, K., & Barlat, F. (1999). A general elasto-plastic finite element formulation based on incremental deformation theory for planar anisotropy and its application to sheet metal forming. *International Journal of Plasticity, 15*(1), 35–67.
11. Tong, W. (2016). Generalized fourth-order Hill's 1979 yield function for modeling sheet metals in plane stress. *Acta Mech., 227*, 2719–2733.
12. Szwed, A., Kamińska, I. (2021). Explicit form of yield conditions dual to a class of dissipation potentials dependent on three invariants. *Acta Mechanica, 232*(3), 1087–1111.
13. Barlat, F., Brem, J. C., Yoon, J. W., Chung, K., Dick, R. E., Lege, D. J., & Chu, E. (2003). Plane stress yield function for aluminum alloy sheets part 1: Theory. *International Journal of Plasticity, 19*(9), 1297–1319.
14. Banabic, D., Aretz, H., Comsa, D. S., & Paraianu, L. (2005). An improved analytical description of orthotropy in metallic sheets. *International Journal of Plasticity, 21*(3), 493–512.
15. Banabic, D., Comsa, D. S., Sester, M., Selig, M., Kubli, W., Mattiasson, K., Sigvant, M. (2008). Influence of constitutive equations on the accuracy of prediction in sheet metal forming simulation. In: *Numisheet*. pp. 37–42.
16. Cazacu, O., & Barlat, F. (2004). A criterion for description of anisotropy and yield differential effects in pressure-insensitive metals. *International Journal of Plasticity, 20*(11), 2027–2045.
17. Stoughton, T. B. (2002). A non-associated flow rule for sheet metal forming. *International Journal of Plasticity, 18*(5), 687–714.
18. Stoughton, T. B., & Yoon, J. W. (2004). A pressure-sensitive yield criterion under a non-associated flow rule for sheet metal forming. *International Journal of Plasticity, 20*(4), 705–731.
19. Stoughton, T. B., & Yoon, J. W. (2006). A review of Drucker's postulate and the issue of plastic stability in metal forming. *International Journal of Plasticity, 22*, 391–433.
20. Stoughton, T. B., & Yoon, J. W. (2008). On the existence of indeterminate solutions to the equations of motion under non-associated flow. *International Journal of Plasticity, 24*, 583–613.
21. Stoughton, T. B., & Yoon, J. W. (2009). Anisotropic hardening and non-associated flow in proportional loading of sheet metals. *International Journal of Plasticity, 25*, 1777–1817.
22. Cvitanic, V., Vlak, F., & Lozina, Z. (2008). A finite element formulation based on non-associated plasticity for sheet metal forming. *International Journal of Plasticity, 24*, 646–687.
23. Safaei, M., Zang, S., & l., Lee, M.G., Waele, W. D. . (2013). Evaluation of anisotropic constitutive models: Mixed anisotropic hardening and non-associated flow rule approach. *International Journal of Mechanical Sciences, 73*, 53–68.
24. Lee, E. H., Stoughton, T. B. Y., & J. W. . (2017). A yield criterion through coupling of quadratic and non-quadratic functions for

anisotropic hardening with non-associated flow rule. *International Journal of Plasticity, 99*, 120–143.

25. Lee, E. H. (2018). Kinematic hardening model considering directional hardening response. *International Journal of Plasticity, 110*, 145–165.

26. Lee, E. H., Choi, H. S., Stoughton, T. B. Y., & J. W. . (2019). Combined anisotropic and distortion hardening to describe directional response with Bauschinger effect. *Int. J. Plasticity, 122*, 73–88.

27. Lee, E. H., & Rubin, M. B. (2020). Modeling anisotropic inelastic effects in sheet metal forming using microstructural vectors–Part I: Theory. *Int. J. Plast, 134*, 102783.

28. Hollenstein, M., Jabareen, M., Rubin, M.B., (2013). Modeling a smooth elastic–inelastic transition with a strongly objective numerical integrator needing no iteration. *Computational Mechanics, 52*, 649–667.

29. Chung, K., Richmond, O. (1992). Ideal forming – I. homogeneous deformation with minimum plastic work. *International Journal of Mechanical Sciences, 34*(7), 575–591.

30. Ting, T. C. T. (1985). Determination of C1/2, C -1/2 and more general isotropic tensor functions of C. *Journal of Elasticity, 15*, 319–323.

31. Tong, W. (2018). Calibration of a complete homogeneous polynomial yield function of six degrees for modeling orthotropic steel sheets. *Acta Mechanica, 229*, 2495–2519.

32. Tian, H., Brownell, B., Baral, M., & Korkolis, Y. P. (2016). Earing in cup-drawing of anisotropic Al-6022-T4 sheets. *International Journal of Material Forming, 10*(3), 329–343.

Jae-Hyuk Lim has been studying as a Ph. D candidate in the department of mechanical engineering in Sungkyunkwan university since 2020. His research field is about the development of yield function based on the anisotropic behavior for sheet metal. And also he has been further extending to the analysis on the extreme mechanical property on sheet metal trimming process considering high rate and temperature.

Eun-Ho Lee is a faculty of the school of Mechanical Engineering in Sungkyunkwan University. He received the Ph.D. degree from the department of mechanical engineering of KAIST in 2015, and has been studying the theory of mechanics for scientific study and engineering applications.